Biogeosciences Discuss., 12, 7671–7703, 2015
www.biogeosciences-discuss.net/12/7671/2015/
doi:10.5194/bgd-12-7671-2015

Biogeosciences Discussions
Open Access

Age depth-model for the past 630 ka in Lake Ohrid (Macedonia/Albania) based on cyclostratigraphic analysis of downhole gamma ray data

H. Baumgarten[1], T. Wonik[1], D. C. Tanner[1], A. Francke[2], B. Wagner[2], G. Zanchetta[3], R. Sulpizio[4], B. Giaccio[5], and S. Nomade[6]

[1]Leibniz Institute for Applied Geophysics, Hannover, Germany
[2]University of Cologne, Institute for Geology and Mineralogy, Cologne, Germany
[3]University of Pisa, Dipartimento di Scienze della Terra, Pisa, Italy
[4]University of Bari Aldo Moro, Dipartimento di Scienze della Terra e Geoambientali, Bari, Italy
[5]Instituto di Geologia Ambientale e Geoingegneria – CNR, Roma, Italy
[6]Laboratoire des Sciences du Climat et de l'Environnement, IPSL, laboratoire CEA/CNRS/UVSQ, Gif-Sur-Yvette, France

Received: 18 February 2015 – Accepted: 13 April 2015 – Published: 22 May 2015

Correspondence to: H. Baumgarten (henrike.baumgarten@liag-hannover.de)

Published by Copernicus Publications on behalf of the European Geosciences Union.

Abstract

We report the gamma ray fluctuations from downhole logging data obtained in the sediments of Lake Ohrid from 0 to 240 m below lake floor. These variations in gamma ray and potassium values strongly correlate with fluctuations in global $\delta^{18}O$ values and can be thus considered a reliable proxy to depict glacial–interglacial cycles, with high clastic input during cold and/or drier periods and high carbonate precipitation during the warm and/or humid periods in Lake Ohrid. Spectral analysis (sliding window) was applied to investigate the climate signal and their evolution over the length of the borehole. Linking the downhole logging data with orbital cycles was used to estimate sedimentation rates, which shift from 45 cm ka^{-1} between 0 to 110 m to 30 cm ka^{-1} from 110 to 240 m below lake floor. The effect of compaction was compensated for. Sedimentation rates increase on average by 14 % after decompaction of the sediment layers. Tuning of minima and maxima in gamma ray and potassium values vs. LR04 minima and maxima, in combination with eight independent tephrostratigraphical tie points, allows the establishment of a robust age model for the downhole logging data over the past 630 ka in Lake Ohrid.

1 Introduction

Lake Ohrid is located at the border between the former Yugoslav Republic of Macedonia (FYROM) and Albania (40°70′ N, 20°42′ E) in the Central Mediterranean region (Fig. 1). It is considered as one of the oldest, continuously-existing lakes worldwide. Its sediments are assumed to contain the climate history over more than one million years and numerous endemic species have evolved in Lake Ohrid. Several pre-site studies between 2004 and 2012 (e.g. multichannel seismic and shallow coring) demonstrated the potential of Lake Ohrid to yield a complete and continuous paleoclimatic record (e.g., Wagner et al., 2008; Lindhorst et al., 2015). A successful deep drilling campaign by the International Continental Scientific Drilling Program (ICDP) was performed in

BGD
12, 7671–7703, 2015

2013. At the main drill site, the "DEEP site" in the central deep basin of Lake Ohrid (Fig. 1), multiple coring and downhole logging tools were applied. Hydroacoustic data obtained by multichannel airgun and sediment echosounder seismics revealed undisturbed sediments as well as certain high amplitude reflectors, which were interpreted as tephra layers (Lindhorst et al., 2015).

The reconstruction of Lake Ohrid's climatic, tectonic and evolutionary biological history, is one of the key objectives of the Scientific Collaboration on Past Speciation Conditions in Lake Ohrid (SCOPSCO) project. This requires a reliable temporal framework of the biotic and abiotic events and thus the establishment of a robust age depth-model. This can be achieved by tephrostratigraphy (Sulpizio et al., 2010; Vogel et al., 2010c), the use of radiometric ages (e.g. from dating of volcanic material in the cores), or by tuning proxy data (e.g. δ^{18}O or TOC) to reference records (Lang and Wolff, 2011; Stockhecke et al., 2014a). Suitable material for independent dating (e.g. well-preserved and coarse-grained tephra layers) is often rare in sediments or hard to detect. Even if age control points are available, changes in the sedimentation rate between these points is uncertain. Amongst proxy data, the effect of global climate signals (Milanković cycles; Milanković, 1920) can be used to construct the temporal framework of a sedimentary record (Batenburg et al., 2012; Prokopenko et al., 2006; Wu et al., 2012). These cycles have periodicities of 100 ka (eccentricity; E), 41 ka (obliquity; O), 23 and 19 ka (precession; P_2, P_1) and determine the intensity of the solar insolation on Earth, whereas their effect is non-uniform and depends on the location of a certain site (e.g. the effect of O is strongest at polar regions) (Pälike, 2005). The 100 ka cycle dominates the past *c*. 900 ka (Berger and Loutre, 2010), which is evident in sedimentary records and strongly imprinted in the widely-used global climate reference record (LR04-stack from benthic foraminifera δ^{18}O) (Lisiecki and Raymo, 2005, 2007). To apply cyclostratigraphic methods successfully, generation and preservation of cycles is required, as well as their continuous recording. Such conditions are favoured in marine environments and ice cores, which are commonly used to analyse cyclicities (Barthes et al., 1999; Golovchenko et al., 1990; Jarrard and Arthur, 1989; Jouzel et al., 2007; Molinie and

BGD
12, 7671–7703, 2015

Ogg, 1990a). However, several lacustrine sequences have recorded global climate signals and have been used for cyclostratigraphic studies (Baumgarten and Wonik, 2014; Bogota-A et al., 2011; Nowaczyk et al., 2013; Prokopenko et al., 2006). Whereas the majority of studies were performed on proxies from sediment cores (e.g. $\delta^{18}O$, organic matter or pollen), analysis of physical properties from downhole logging have been proven successful (Barthes et al., 1999; Golovchenko et al., 1990; Jarrard and Arthur, 1989; Molinie and Ogg, 1990b; Wonik, 2001).

Physical in-situ properties (e.g. seismic velocity or spectral gamma ray) can be only achieved by downhole logging methods and provide a first data set that is available within hours after the tools are run in hole. Contrasting physical properties and therefore changes in the sediment characteristics (e.g. sedimentological composition, grain size) can trigger cyclic changes in the logging data (Baumgarten and Wonik, 2014; Kashiwaya et al., 1999; Paulissen and Luthi, 2011; Scholz et al., 2011). Such cyclic changes can be potentially revealed by applying cyclostratigraphic methods. The aim of this study is the generation of a robust age depth-model down to 240 m below lake floor (mblf) by an integrated study of downhole data with tephrostratigraphic age control from the sediment cores. Special emphasis is given to the effect of compaction and its subsequent impact on estimates of sedimentation rates. Furthermore, the response of the physical in-situ properties from spectral gamma ray (contents of potassium, thorium and uranium) and their application as proxy for changing environmental conditions in the catchment area is investigated.

2 Setting and sediment dynamics of Lake Ohrid

Lake Ohrid is located on the Balkan Peninsula at an altitude of 693 m above sea level in a northwest-trending active tectonic graben. It is considered to have formed within a 1st stage (Late Miocene) as a pull-apart basin and a 2nd stage (Pliocene) of extensional movement (E–W extension) which led to the recent geometry (Lindhorst et al., 2015). The lake is considered be the oldest continuously-existing lake in Europe, as supported

BGD
12, 7671–7703, 2015

by molecular clock analysis that estimate the onset of the lake formation to 1.5 to 3 million years (Ma) (Trajanovski et al., 2010; Wagner et al., 2014).

Lake Ohrid has a surface area of 360 km^2 and a water depth up to 290 m. The water originates mainly from karst inflows (50 %), precipitation (25 %), and river and surface runoff (25 %), whereas the karst springs are primarily fed by the 150 m higher "sister lake" Prespa (Wagner et al., 2014). The recent local climate is characterized by warm dry summers (mean temperature 26 °C) and cold winters (−1 °C). The annual precipitation is about 750 mm and the winds are prevailing southerly or northerly, which is topographically controlled by the shape of the lake valley (Vogel et al., 2010a). Due to its downwind location of most of the Quaternary volcanoes of central-southern Italy, Lake Ohrid's sediments can provide a record of the volcanic history of the northern Mediterranean region (Sulpizio et al., 2010). The oligotrophic lake houses an extraordinary number of endemic species (> 200, e.g. ostracodes) and it is therefore considered to be a hotspot to study the evolution of the various species (Albrecht and Wilke, 2008). The catchment area southeast and northwest of the lake mostly consists of Triassic carbonates and clastics, whereas ophiolites (nickel, iron and chromium-bearing) are exposed on the western and southwestern shore (Vogel et al., 2010b). The sediment dynamics for the past 150 ka have been investigated by up to 15 m long sediment cores from different marginal parts of the lake basin (e.g. Wagner et al., 2008; Belmecheri et al., 2009; Vogel et al., 2010a). To simplify, two major lithofacies can be distinguished: (A) sediments with high detrital clastic content with no or very low carbonate content, together with low total organic matter and few diatoms, and (B) sediments with high content of carbonates, abundant ostracodes, small clastics and high organic matter. Lithofacies A is associated with glacial conditions (Marine Isotope Stages; MIS 2, 4, 6), high clastic supply and low lake productivity, whereas lithofacies B formed during interglacial conditions (mainly during MIS 1 and 5), with high lake productivity and formation of authigenic carbonates. Age control of the sediments was obtained by radiocarbon dating and tephrochronology.

BGD
12, 7671–7703, 2015

3 Methods and background

3.1 Downhole logging data acquisition and processing

The multiple-cored DEEP site has six boreholes (A to F), of which holes A and E only cover the uppermost few meters of the sediment succession. Each of the deeper holes was drilled with a diameter of 149 mm and water-based mud was used to clean the holes from cuttings and to stabilize the side walls during the coring process. Hole C was logged immediately after drilling down to 470 mblf, and amongst other probes (e.g. resistivity and borehole televiewer), spectral gamma ray (SGR) and sonic were used. To prevent the unconsolidated sediments caving in, the SGR probe was run through the drillpipe and a continuous record of the sediments down to 470 mblf was achieved. The SGR data was acquired using the SGR 70-slimhole tool of the Leibniz Institute for Applied Geophysics (LIAG), which records the total gamma radiation (GR), as well as the spectral components (potassium; K, thorium; Th and uranium; U) and their contribution to the GR. The tool was run with a logging speed of 3 m min^{-1} and a sampling rate of 10 cm. The achievable minimum bed resolution is controlled by the size of the BGO crystal (5 cm × 15 cm) and the characteristics of the target formation (e.g. the absolute value range and contrast of values between neighbouring beds) (Theys, 1991). The vertical resolution can be estimated at 15–20 cm. The sonic tool, which measures the seismic velocity (Vp), was applied afterwards at a speed of 4 m min^{-1} and a depth increment of 10 cm. To allow open hole logging by sonic, the drillpipes were successively pulled upwards until open hole sections of c. 50 m were accessible. The uppermost 30 mblf could not be logged by the sonic tool, because some drillpipes were kept in hole to allow other probes to enter. The measuring principles are described by Rider and Kennedy (2011) and the tools are specified in Buecker et al. (2000) and Barrett et al. (2000). The data was acquired, preprocessed and processed with the software GeoBase® (Antares, Germany) and WellCAD® (Advanced Logging Technology, Luxembourg).

BGD
12, 7671–7703, 2015

3.2 Sliding window method

Sedimentary cycles in lake records can be studied by cyclostratigraphic methods for a potentially orbital driven origin (Lenz et al., 2011; Prokopenko et al., 2001; Weedon, 2003). To investigate wavelengths and amplitude of the contained signals, fast Fourier transform (Weedon, 2003) can be used. The sliding window method (≡ windowed Fourier transform) (Baumgarten and Wonik, 2014; Molinie and Ogg, 1990b; Torrence and Compo, 1998; Weedon, 2003) can be applied to identify the distribution of cycles within a series and their evolution over the dataset: the spectral analysis is calculated for a depth interval of specific length (window size) and the resulting spectrum is allocated to the centre of the window. Subsequently, the window is moved downwards by a certain step size and the analysis is repeated at consecutive depth positions until the window border reaches the end of the dataset. The results are presented in a three-dimensional spectrogram with colour-coding of the relative power of the different frequency components. Generally, a small window size is favourable to maximize the length of the resulting plot. However, the contained cycle needs to be covered and cannot be determined if the window size was chosen too short, e.g. only half the signal's wavelength. The optimal window size can be determined by empirical testing. Spectral analysis for identification of the characteristic periodicities (Jenkins and Watts, 1969; Priestley, 1981) was performed on normalized SGR data using fast Fourier Transform within MATLAB (MathWorks®).

The detection of cycles by SGR logging is limited by the Nyquist Frequency (twice the sampling rate) (Molinie and Ogg, 1990a). The temporal resolution can be estimated by the vertical resolution of the applied tools (minimum bed resolution of the SGR tool of 15–20 cm; Sect. 3.1) and the averaged sedimentation rate. For a mean sedimentation rate of e.g. 38 cm ka^{-1}, cycles in the range of 0.8 to 1.1 ka are resolvable by SGR logging.

BGD
12, 7671–7703, 2015

3.3 Depth matching of downhole logging and core data

In this work, downhole logging data, in conjunction with age control points from tephra layers, is used to construct an age depth-model. Therefore, matching of core and logging depth is required. To provide age control by distinct tephra layers, they need to be identified in the cores by visual description or by their physical properties (e.g. susceptibility from core logging) in contrast to the background sedimentation. Artifacts in the coring process as incorrect depth allocation of coring tools or gas extension of sediments after cores are on deck and pressure release produce erroneous depth. Furthermore, depth shifts between core and logging depth are generated because the downhole data originates from one hole (C; down to 470 mblf) and the core composite record (see Francke et al., 2015) is composed of four different holes (Sect. 3.1) which are tens of metres apart. The depth of a distinct sediment layer may differ up to 3 to 4 m between these holes. The matching of borehole logging data and sediment core is described in detail in Francke et al. (2015) and is based on a correlation of K-contents from SGR with K-intensities from XRF-scanning, and using magnetic susceptibility from downhole logging and Multi Sensor Core Logging (MSCL) on sediment cores. Trends and patterns were compared and preferred over correlation of (single) small-scaled features in the data. Cross correlation was used to prevent systematic depth shifts of these data sets and for quality control.

3.4 Compaction

To perform cyclostratigraphic studies and to estimate an age depth-relationship and sedimentation rates, compaction and associated reduction of sediment thickness due to overburden pressure must be considered. The original (decompacted) thickness of the sediments can be calculated if the initial (surface) porosity and the compaction coefficient (Brunet, 1998) can be determined. The amount of porosity decrease with greater depth depends on sediment properties, e.g. grain size and sorting (Serra and

BGD
12, 7671–7703, 2015

Serra, 2003) and can be expressed as:

$$\phi(z) = \phi_0 \times e^{(-cz)} \quad (1)$$

where the porosity (ϕ) at a specific depth (z) is to be estimated; ϕ_0 is the initial porosity and c is the compaction coefficient (Athy, 1930; Brunet, 1998). Whereas porosity can be measured directly on the sediment cores, e.g. by Archimedean weighing, the physical properties, in particular from (unconsolidated) sediment cores are typically disturbed due to drilling, release of pressure, and core handling. Therefore, measurements by downhole logging are more suitable; in-situ porosity can be gained by neutron porosity logging or derived, e.g. from bulk density. These tools operate with radioactive methods and the import procedure into foreign countries is usually extremely complicated and seldom successful. Therefore, the radioactive tools from the LIAG could not be used at Lake Ohrid. However, porosity was derived by an empirical relationship from sonic data (Vp) (Erickson and Jarrard, 1998), which were recorded continuously from below 30 mblf. The software 2-DMove® (Midland Valley Exploration Ltd.) was used to decompact the sediments and calculate the original sediment thickness.

4 Results

4.1 Selection of SGR data

The output curves from SGR were compared to estimate the contribution of the spectral components to the total gamma ray. GR is mainly controlled by K and Th, which develop uniformly ($R > 0.9$). GR and K were used for further investigations, whereas K was chosen over Th, because it is also available from XRF core scanning and the interpretation can be reviewed easily.

BGD
12, 7671–7703, 2015

4.2 Correlation of GR with the global climate reference $\delta^{18}O$ record

The downhole logging data (GR and K) between 0 m and 240 mblf was compared to the global benthic isotope stack LR04 stack (Lisiecki and Raymo, 2005). In order to select an appropriate temporal window we considered the current age estimates from tephra dating (eight age depth-points; Table 1). After the anchor points from tephra deposits were defined, significant variations in the data were correlated; a very similar cyclicity with a positive correlation between GR and K from downhole logging data and $\delta^{18}O$ data was observed (Fig. 2a). The onset and terminations of several MIS stages can be easily distinguished in the downhole logging data, whereas warm and/or humid periods (decreased $\delta^{18}O$ values) correlate with low GR values. 30 additional tie points (Table 1) were set due to the strong similarities between the curves characteristics. After matching these tie points, high correlation of both datasets ($R = 0.75$) was observed. The tephra ages and tie points from correlation between GR, K and LR04 were used to assign a (preliminary) age scale to the data (Fig. 2b). Within the data, the age scale between the tie points was generated by linear interpolation. According to the established age model, the 240 m long sediment succession covers a time period between ca. 630 ka (including MIS 15) and the present.

The conspicuous similarity of the datasets allows calculation of a synthetic $\delta^{18}O$-curve from GR by a simple regression of both datasets. Therefore, normal-distributed data is required and thus the prominent tephra layers at 20 and 68 mblf (Fig. 2c) were considered to be outliers and removed. Best results were achieved by a linear solution ($R^2 = 0.60$) as follows:

$$\delta^{18}O_{calc}(‰) = 3.19 + 0.03 \times GR(gAPI). \quad (2)$$

Whereas cycles and trends are similar in both datasets, the amplitudes between the LR04 stack and the synthetic $\delta^{18}O$ (derived from GR; $\delta^{18}O_{calc}$; Fig. 2c) are not completely matched. The $\delta^{18}O_{calc}$ values from 630 to 430 ka are lower than compared to LR04. From 430 to 185 ka the amplitude of $\delta^{18}O_{calc}$ is higher and during the past

BGD
12, 7671–7703, 2015

185 ka, $\delta^{18}O_{calc}$ is mostly decreased compared to LR04. These three zones are indicated in Fig. 2c.

4.3 Spectral characteristics of GR data, temporal evolution and sedimentation rates

After visual comparison of GR and K and LR04 and the observed strong correlation of periods with low GR and K and warm and/or humid periods, spectral analysis by sliding window method (Sect. 3.2) was applied to objectively identify the possible cycles and their temporal distribution. The spectral analysis was calculated with a window of 90 m length and a step size of 1 m. Thus, the stepwise calculation for the depth section from 0 to 240 mblf and the resulting three-dimensional spectral plot (Fig. 3) is composed of 150 spectra. The plot ranges from 45 to 240 mblf, because the first spectrum is allocated to the window centre (Sect. 3.2) and therefore, half of the window length is not displayed. Two prominent spectral peaks are evident in the dataset, as indicated by colour. These spectral peaks have wavelengths of 30 and 45 m (Fig. 3). The distribution of the cycles is non-uniform over the dataset and a break in the spectral characteristics occurs at about 110 mblf. Based on the reduced relative power of the 30 m signal and the subsequent increased power of the 45 m frequency at 110 mblf, the plot can be split in a lower interval (I) and an upper interval (II) (Fig. 3). Two single spectra from depths of 170 and 50 mblf are displayed in Fig. 3. The similar cyclicity in the LR04 stack and GR (Fig. 2a, b) suggests that the 100 ka cycle, known as dominant periodicity in sedimentary archives for the past ca. 900 ka and clearly written in the $\delta^{18}O$ data, has the strongest effect on the cyclic characteristics of the GR data. The highest amplitudes were therefore linked to the 100 ka cycle. Averaged sedimentation rates can be calculated using this link (45 m ≡ 100 ka cycle), for 110 to 0 mblf as follows:

$$\frac{45\,\mathrm{m}}{100\,\mathrm{ka}} = 45\,\mathrm{cm\,ka^{-1}}. \quad (3)$$

BGD
12, 7671–7703, 2015

Furthermore, the time of deposition can be estimated by using this rate and the length of the interval II (length of 110 m):

$$\frac{110\,\mathrm{m}}{45\,\mathrm{cm\,ka^{-1}}} = 244\,\mathrm{ka}. \quad (4)$$

The sedimentation rate for interval I (length of 130 m) can be calculated as 30 cm ka^{-1} (30 m ≡ 100 ka cycle) which gives an overall time of deposition (sum of interval I and II) of 677 ka.

The sedimentation rates from sliding window show a distinct shift from 30 to 45 cm ka^{-1} at ca. 110 mblf (Fig. 4). However, the sedimentation rates from visual tying are much more variable and range from 22 to 71 cm ka^{-1}. Exceptionally high sedimentation rates occurred during MIS 6 and lowest sedimentation rates occurred during MIS 11 and 13.

4.4 Decompaction of the pelagic sediments and subsequent spectral analysis on stretched GR data

The effect of decreased sediment thicknesses due to compaction over time was determined to investigate its impact on the estimates of sedimentation rates. The Vp data from sonic logging was used to derive porosity after Erickson and Jarrard (1998). The porosity values were averaged for layers of 100 m thickness (Fig. 5a). The initial porosity (ϕ_0) was determined at 80 % and the compaction coefficient was estimated at 0.39 km^{-1}. These parameters were used as input data for modeling decompaction of the sediments, and the 2-D model was calculated for layers of 50 m thickness. The modeling process starts with the removal of the top layer and subtraction of its overburden pressure. The new thicknesses of the lowermost layers are thereafter calculated and these steps were repeated again downwards. The resulting thicknesses of the sediment layers after decompaction show a quasi-linear increase with greater depth for these small depths (Fig. 5b). The decompaction of the sediment layers ranges from

BGD
12, 7671–7703, 2015

10 to 30 % downwards and the cumulative thickness of the sediment sequence (present thickness of 240 m) is increased by 36 m (to 276 m).

The GR data was stretched (Fig. 5c) and subsequently spectrally analyzed by sliding window (Fig. 5d) to determine the effect of decompaction on the spectral analysis. The spectral analysis shows two spectral peaks (Fig. 5d; wavelength of 36 m from 276 to 118 m and wavelength of 48 m from 118 to 0 m). Linking these spectral peaks to the 100 ka cycle provided sedimentation rates of 36 cm ka^{-1} for interval I and 48 cm ka^{-1} for interval II. Times of deposition are 433 ka for interval I and 244 ka for interval II, respectively.

5 Discussion

5.1 Response of GR to the global climate over the past 630 ka

The strong correlation of GR and K with LR04 (low GR and K during warm and/or humid periods, high in cold and/or drier periods) suggest a response of the sedimentary system to the temperature and hydrological changes related to the global ice-volume fluctuations of the glacial–interglacial cycles. The fluctuations are likely to be controlled by the input and deposition of clastics (K and Th sources), which are suggested to have increased during the past ca. 136 ka, when glacial conditions prevailed (except MIS 1 and 5e) at Lake Ohrid (Vogel et al., 2010a). In particular, the reduced input of organic matter and calcium carbonate during cold and/or drier periods seems to amplify the enhanced input of clastic material. During warm and/or humid periods, carbonate production and preservation is increased (Vogel et al., 2010a). In combination with higher organic matter flux, the clastic content of the sediments is reduced and the GR and K data is lower. Either the total content of clastics is lower during warm-humid periods or the amount is decreased relatively to carbonate (and organic matter). However, as discussed by Vogel et al. (2010a), less vegetation cover during cold-drier periods is likely and also suggests increased erosion in the catchment and subsequent higher input

BGD
12, 7671–7703, 2015

of clastic material. Based on our interpretation, these dynamics of a cyclic change of carbonate-rich and clastic-rich sedimentation were constant at least for the past 630 ka, as evident in the GR and K data.

Three zones were observed, based on difference in the amplitude between the synthetic δ^{18}O curve from GR (δ^{18}Ocalc) and the referenced record: (A) 630 to 430 ka (MIS 15 to MIS 12), (B) 430 to 185 ka (MIS 11 to MIS 7) and, (C) 185 to 0 ka (MIS 6 to MIS 1). The comparison of the synthetic $\delta^{18}O_{calc}$ to the LR04 revealed systematically lower values in zones (A) and (C) and higher values in zone (B). Under the assumption that our data reflects prevailing climate-driven fluctuations in the sediments, the differences between the $\delta^{18}O_{calc}$ and LR04 could indicate deviations from a linear response to the global ice-volume fluctuations. Therefore, the suggested climate signal would not completely be in line with the global climate variations and be more variable even on glacial–interglacial scale. Furthermore, local environmental processes (e.g. variations in the catchment area due to topographic changes and subsequent supply of clastics) might have additionally affected the sediment properties. The (few) tephra deposits have contributed to the characteristics of the data as well; the tephra layers can be recognized in the K data and have shaped the curve, in addition to the climate-dependent deposition of clastics.

The matching of the GR and K data with the global climate reference record equates the timing of the climate dynamics recorded in the oceans to Lake Ohrid. This means that if the downhole logging data is tied to this age scale, differences between the response times of Lake Ohrid and the global climate trend (e.g. onset of terminations) could be lost. However, even if the comparable small system was likely to be subject to faster climate response compared to records from marine sediments, the correlation with the global signal and the resulting age depth-model can be still verified in large parts (down to 206 mblf) by tephrochronology. Further interpretation of the complete dataset was postponed to allow integrated investigation of cyclostratigraphic analysis with age control from cores.

BGD
12, 7671–7703, 2015

5.2 Sedimentation rates: major trends, small-scale fluctuations and the effect of compaction

The relative power of the spectral peaks from sliding window analysis seems to decrease towards the top (wavelength of 45 m; starting from interval II). The strength of the signal depends on the number of cycles that are detected by spectral analysis. The 45 m long cycle can be contained up to 2.4 times in the 110 m long interval II, whereas the cycle of wavelength of 30 m might be recorded more frequently in the 130 m long interval (I). This might contribute to the higher intensity of the 30 m amplitude and thus we cannot interpret this as stronger cyclicity in the lower part.

Based on sliding window analysis the sedimentation rates are constant (30 cm ka^{-1}) for a long period of time (433 ka), apart from a shift to increased rates at about 110 mblf to 45 cm ka^{-1}. However, small-scale variations in these rates cannot be resolved due to averaging and the used window of 90 m length. More variable results are indicated by tying of GR and K to LR04.The sedimentation rates are generally lower from MIS 15 to MIS 9 (average of 32 cm ka^{-1}) and higher from MIS 8 to 1 (average of 48 cm ka^{-1}). The lowest rates (22 cm ka^{-1}) occur during MIS stages 13, 11 and 9. Strongly-increased sedimentation rates (71 cm ka^{-1}) occur during MIS 8 and in particular during MIS 6. Therefore, a tendency of decreased sedimentation rates during interglacials and increased rates during glacial periods can be derived. Even if these fluctuations do not correlate with all of the MIS stages, it seems to be coupled to glacial–interglacial dynamics in large parts. This trend suggests higher accumulation of clastic-rich glacial deposits compared to calcium carbonate-rich deposition during interglacials. The overall trend from lower rates in the bottom part (> 110 mblf, sliding window; > 130 mblf; LR04 tie points) to increased values towards the top is comparable.

The cumulative time of deposition based on these rates and the corresponding sediment thicknesses range from 630 ka (visual tie points) to 677 ka (sliding window) and are in a similar range (Fig. 6). We consider the estimated time of deposition from the tuning to LR04 to be of higher accuracy than compared to the averaged estimates from

BGD
12, 7671–7703, 2015

sliding window. The agreement with results from cores (Francke et al., 2015) supports the age depth-model in addition. Nonetheless, the sliding window method is proven useful to estimate averaged sedimentation rates and complements the results of the cyclic characteristics of the data. Whereas age control from tephrochronology is only available only down to 206 mblf, the interpretation was extended down to 240 mblf based on the constant cyclic characteristics at these depths. The averaged sedimentation rates from sliding window (30 cm ka^{-1}) agree with the rates from tuning to LR04 (mean of 32 cm ka^{-1}).

The required initial porosity for modeling of the effect of compaction was derived from sonic logging (ϕ_0 = 80 %) and is commonly lower (at ca. 65 %) for sedimentary basins. Studies of physical properties of marine sediment cores have shown comparable value ranges for seafloor deposits (ϕ = 80 %, Vp = 1540 m s^{-1}; Kim and Kim, 2001) and even higher porosity values (> 80 %; Kominz et al., 2011) for unconsolidated sediments. The compaction coefficient c was estimated at 0.39 km^{-1} and lies in a value range between that used for sands (0.20 km^{-1}) and carbonates (0.50 km^{-1}) and thus is considered reasonable. The overall trend of a quasi-linear evolution of decompaction with increasing depth was observed, although Eq. (1) describes an exponential curve, it can be approximated to a line over short (< 500 m) lengths. This is in accordance with the average linear increase of Vp with greater depth. The tephra layers, with only few cm thicknesses, are considered to have little impact on the compaction of the sediments.

The spectral analysis on the stretched data set revealed a very similar spectral characteristic compared to the sliding window plot of the compacted data. However, the two spectral peaks (wavelengths of 30 and 45 m) are shifted to higher wavelengths and increased to wavelengths of 36 m (interval I) and 48 m (interval II). Therefore, the sedimentation rates are increased accordingly and would be underestimated by 7 to 20 %, if they are not corrected for the effect of compaction. To estimate the time of deposition, two input quantities were used: (1) the sedimentation rates and, (2) the thickness of the sediment layer for which they apply. Due to the stretching of the dataset, the resulting sedimentation rates, as well as the length of the intervals are increased and

BGD
12, 7671–7703, 2015

thus the time of deposition remains unchanged. Therefore, the effect of compaction on this calculation is neglectable.

6 Conclusions

Can climatic indicators be derived from downhole logging, despite its limited vertical (and temporal) resolution and can these proxies be used to reconstruct a robust age depth-model?

The strong response to the global climate signal (LR04) suggests that the K (and Th) content reflects a cyclic change of undisturbed, continuous sedimentation and thus that the conditions were constant over a long period of time and prevailing in balance with the global climate. To investigate the response of our data to the global climate trend, a synthetic δ^{18}O-curve was generated that reveals minor deviations. The deviations could indicate either that the local climatic conditions were not fully in line with the global climate or, that local processes in the sedimentary system changed over time.

Within two independent attempts, visual tying to the global reference LR04 record as well as spectral analysis by sliding window method, and linking of high amplitudes to orbital cycles, a similar result was achieved. To derive sedimentation rates from sliding window method, the effect of compaction must be taken into account. The use of the present thicknesses of the sediment layers underestimates sedimentation rates by an average 14 % and these needs to be corrected for by decompaction.

In conjunction with tephrochronology from core material, a robust age depth-relationship can be created. This data set will play a crucial role for other working groups and will complement the age depth-model from core analysis. Their combination will provide the temporal framework (e.g. for refining of the seismo-stratigraphical model by Lindhorst et al., 2015) and will there within contribute to the reconstruction of Lake Ohrid's climatic, tectonic and evolutionary biological history and answer the main questions of the SCOPSCP project.

BGD
12, 7671–7703, 2015

Due to the successful construction of an age depth-model based on the GR and K data down to 240 mblf, we are optimistic that the complete lacustrine sediment succession (down to 433 mblf) has high potential for cyclostratigraphic analysis and will provide a key component to determine Lake Ohrid's temporal framework.

Acknowledgements. The SCOPSCO Lake Ohrid drilling campaign was funded by ICDP, the German Ministry of Higher Education and Research, the German Research Foundation, the University of Cologne, the British Geological Survey, the INGV and CNR (both Italy), and the governments of the republics of Macedonia (FYROM) and Albania. Logistic support was provided by the Hydrobiological Institute in Ohrid. Drilling was carried out by Drilling, Observation and Sampling of the Earth's Continental Crust's (DOSECC) and using the Deep Lake Drilling System (DLDS). Special thanks are due to Beau Marshall and the drilling team. Ali Skinner and Martin Melles provided immense help and advice during logistic preparation and the drilling operation.

We thank the German Research Foundation for financial support (WO 672/10-1) for the downhole logging. The acquisition of these high quality data was only possible due to the great commitment of our technical staff Thomas Grelle and Jens Kuhnisch.

References

Albert, P. G., Hardiman, M., Keller, J., Tomlinson, E. L., Smith, V. C., Bourne, A. J., Wulf, S., Zanchetta, G., Sulpizio, R., Müller, U. C., Pross, J., Ottolini, L., Matthews, I. P., Blockley, S. P. E., and Menzies, M. A.: Revisiting the Y-3 tephrostratigraphic marker: a new diagnostic glass geochemistry, age estimate, and details on its climatostratigraphical context, Quaternary Sci. Rev., in press, doi:10.1016/j.quascirev.2014.04.002, 2014.

Albrecht, C. and Wilke, T.: Ancient lake ohrid: biodiversity and evolution, Hydrobiologia, 615, 103–140, 2008.

Athy, L. F.: Density, porosity, and compaction of sedimentary rocks, AAPG Bull., 14, 1–24, 1930.

Barrett, P. J., Sarti, M., and Wise, S.: Studies from the Cape Roberts Project Ross Sea, Antarctica Initial Report on CRP-3 Terra Antartica, 7, 19–56, 2000.

BGD
12, 7671–7703, 2015

Barthes, V., Pozzi, J. P., Vibert-Charbonnel, P., Thibal, J., and Melieres, M. A.: High-resolution chronostratigraphy from downhole susceptibility logging tuned by palaeoclimatic orbital frequencies, Earth Planet. Sc. Lett., 165, 97–116, 1999.

Batenburg, S. J., Sprovieri, M., Gale, A. S., Hilgen, F. J., Hüsing, S., Laskar, J., Liebrand, D., Lirer, F., Orue-Etxebarria, X., Pelosi, N., and Smit, J.: Cyclostratigraphy and astronomical tuning of the Late Maastrichtian at Zumaia (Basque country, Northern Spain), Earth Planet. Sc. Lett., 359, 264–278, 2012.

Baumgarten, H. and Wonik, T.: Cyclostratigraphic studies of sediments from Lake Van (Turkey) based on their uranium contents obtained from downhole logging and paleoclimatic implications, Int. J. Earth Sci., 1–16, 2014.

Belmecheri, S., von Grafenstein, U., Namiotko, T., Robert, C. M., Andersen, N., Danielopol, D. L., Caron, B., Bordon, A., Regnier, D., Mazaud, A., Sulpizio, R., Zanchetta, G., Grenier, C., Tiercelin, J. J., Fouache, E., and Lezine, A. M.: Potential of Lake Ohrid for long palaeoclimatic and palaeoenvironmental records, the last glacial–interglacial cycle (140 ka), Eos, Transactions, American Geophysical Union, 90, PP14A-03, 2009.

Berger, A. and Loutre, M. F.: Modeling the, 100-kyr glacial–interglacial cycles, Global Planet. Change, 72, 275–281, 2010.

Bogota-A, R. G., Groot, M. H. M., Hooghiemstra, H., Lourens, L. J., van der Linden, M., and Berrio, J. C.: Rapid climate change from north Andean Lake Fuquene pollen records driven by obliquity; implications for a basin-wide biostratigraphic zonation for the last 284 ka, Quaternary Sci. Rev., 30, 3321–3337, 2011.

Brunet, M. F.: Method of Quantitative Study of Subsidence, Oxford and IBH Publishing Company Pvt., New Delhi, India, 79–88, 1998.

Buecker, C. J., Jarrard, R. D., Wonik, T., and Brink, J. D.: Analysis of downhole logging data from CRP-2/2A, Victoria Land Basin, Antarctica, a multivariate statistical approach, Terra Antartica, 7, 299–310, 2000.

De Vivo, B., Rolandi, G., Gans, P. B., Calvert, A., Bohrson, W. A., Spera, F. J., and Belkin, H. E.: New constraints on the pyroclastic eruptive history of the Campanian volcanic Plain (Italy), Min. Pet., 73, 47–65, 2001.

Erickson, S. N. and Jarrard, R. D.: Velocity-porosity relationships for water-saturated siliciclastic sediments, J. Geophys. Res., 30, 385–30, 1998.

Giaccio, B., Arienzo, I., Sottili, G., Castorina, F., Gaeta, M., Nomade, S., Galli, P., and Messina, P.: Isotopic (Sr-Nd) and major element fingerprinting of distal tephras: an appli-

BGD
12, 7671–7703, 2015

cation to the Middle-Late Pleistocene markers from the Colli Albani volcano, central Italy, Quaternary Sci. Rev., 67, 190–206, 2013.
Golovchenko, X., O'Connell, S. B., and Jarrard, R. D.: Sedimentary response to paleoclimate from downhole logs at Site 693, Antarctic continental margin, in: Proceedings of the Ocean Drilling Program, Scientific Results, 113, 239–251, 1990.
Iorio, M., Liddicoat, J., Budillon, F., Incoronato, A., Coe, R. S., Donatella, D., Insinga, D., Cassata, W., Lubritto, C., Angelino, A., and Tamburrino, S.: Combined palaeomagnetic secular variation and petrophysical records to time constrain geological and hazardous events: an example from the eastern Tyrrhenian Sea over the last 120 ka, Global Planet. Change, 113, 91–109, 2013.
Jarrard, R. D. and Arthur, M. A.: Milankovitch paleoceanographic cycles in geophysical logs from ODP Leg 105, Labrador Sea and Baffin Bay, in: Proceedings of the Ocean Drilling Program, Scientific Results, 105, 757–772, 1989.
Jenkins, G. M. and Watts, D. G.: Spectral Analysis and Its Applications, Holden Day, San Francisco, 525 pp., 1969.
Jouzel, J., Masson-Delmotte, V., Cattani, O., Dreyfus, G., Falourd, S., Hoffmann, G., Minster, B., Nouet, J., Barnola, J. M., Chappellaz, J., Fischer, H., Gallet, J. C., Johnsen, S., Leuenberger, M., Loulergue, L., Luethi, D., Oerter, H., Parrenin, F., Raisbeck, G., Raynaud, D., Schilt, A., Schwander, J., Selmo, E., Souchez, R., Spahni, R., Stauffer, B., Steffensen, J. P., Stenni, B., Stocker, T. F., Tison, J. L., Werner, M., and Wolff, E. W.: Orbital and millennial Antarctic climate variability over the past 800,000 years, Science, 317, 793–796, 2007.
Kashiwaya, K., Ryugo, M., Horii, M., Sakai, H., Nakamura, T., and Kawai, T.: Climato-limnological signals during the past 260,000 years in physical properties of bottom sediments from Lake Baikal, J. Paleolimnol., 21, 143–150, 1999.
Kim, G. Y. and Kim, D. C.: Comparison and correlation of physical properties from the plain and slope sediments in the Ulleung Basin, East Sea (Sea of Japan), J. Asian Earth Sci., 19, 669–681, 2001.
Kominz, M. A., Patterson, K., and Odette, D.: Lithology dependence of porosity in slope and deep marine sediments, J. Sediment. Res., 81, 730–742, 2011.
Lang, N. and Wolff, E. W.: Interglacial and glacial variability from the last 800 ka in marine, ice and terrestrial archives, Clim. Past, 7, 361–380, doi:10.5194/cp-7-361-2011, 2011.
Laurenzi, M. A. and Villa, I. M.: $^{40}Ar/^{39}Ar$ chronostratigraphy of Vico ignimbrites, Period. Mineral., 56, 285–293, 1987.

BGD
12, 7671–7703, 2015

Lenz, O. K., Wilde, V., and Riegel, W.: Short-term fluctuations in vegetation and phytoplankton during the middle Eocene greenhouse climate; a 640-kyr record from the Messel oil shale (Germany), Int. J. Earth Sci., 100, 1851–1874, 2011.
Lindhorst, K., Krastel, S., Reicherter, K., Stipp, M., Wagner, B., and Schwenk, T.: Sedimentary and tectonic evolution of Lake Ohrid (Macedonia/Albania), Basin. Res., 27, 84–101, 2015.
Lisiecki, L. E. and Raymo, M. E.: A Pliocene-Pleistocene stack of 57 globally disturbed benthic δ^{18}O records, Paleoceanography, 20, PA1003, doi:10.1029/2004PA001071, 2005.
Lisiecki, L. E. and Raymo, M. E.: Plio-Pleistocene climate evolution; trends and transitions in glacial cycle dynamics, Quaternary Sci. Rev., 26, 56–69, 2007.
Marra, F., Karner, D. B., Freda, C., Gaeta, M., and Renne, P. R.: Large mafic eruptions at the Alban Hills volcanic district (Central Italy): chronostratigraphy, petrography and eruptive behaviour, J. Volcanol. Geoth. Res., 179, 217–232, 2009.
Milanković, M.: Théorie mathématique des phénomènes thermiques produits par la radiation solaire, Gauthier-Villars et Cie, Paris, 1920.
Molinie, A. J. and Ogg, J. G.: Milankovitch cycles in Upper Jurassic and Lower Cretaceous radiolarites of the Equatorial Pacific; spectral analysis and sedimentation rate curves, in: Proceedings of the Ocean Drilling Program, Scientific Results, 129, 529–547, 1990a.
Molinie, A. J. and Ogg, J. G.: Sedimentation-rate curves and discontinuities from sliding-window spectral analysis of logs, Log. Anal., 31, 370–374, 1990b.
Nomade, S., Knight, K. B., Beutel, E., Renne, P. R., Verati, C., Feraud, G., and Marzoli, A.: Duration and eruptive chronology of CAMP; implications for central Atlantic rifting and the Triassic-Jurassic boundary, Eos, Transactions, American Geophysical Union, 86, V13A-0519, 2005.
Nowaczyk, N. R., Haltia, E. M., Ulbricht, D., Wennrich, V., Sauerbrey, M. A., Rosén, P., Vogel, H., Francke, A., Meyer-Jacob, C., Andreev, A. A., and Lozhkin, A. V.: Chronology of Lake El'gygytgyn sediments – a combined magnetostratigraphic, palaeoclimatic and orbital tuning study based on multi-parameter analyses, Clim. Past, 9, 2413–2432, doi:10.5194/cp-9-2413-2013, 2013.
Pälike, H.: Earth, Orbital Variation (Including Milankovitch Cycles), Elsevier Academic Press, Oxford, UK, 410–421, 2005.
Paulissen, W. E. and Luthi, S. M.: High-frequency cyclicity in a miocene sequence of the Vienna Basin established from high-resolution logs and robust chronostratigraphic tuning, Palaeogeogr. Palaeocl., 307, 313–323, 2011.

BGD
12, 7671–7703, 2015

Petrosino, P., Jicha, B. R., Mazzeo, F. C., and Russo Ermolli, E.: A high resolution tephrochronological record of MIS 14–12 in the Southern Apennines (Acerno basin, Italy), J. Volcanol. Geoth. Res., 274, 34–50, 2014a.
Priestley, M. B.: Spectral Analysis and Time Series, Academic Press, New York, 1981.
Prokopenko, A. A., Williams, D. F., Karabanov, E. B., and Khursevich, G. K.: Continental response to Heinrich events and Bond cycles in sedimentary record of Lake Baikal, Siberia, Global Planet. Change, 28, 217–226, 2001.
Prokopenko, A. A., Hinnov, L. A., Williams, D. F., and Kuzmin, M. I.: Orbital forcing of continental climate during the Pleistocene; a complete astronomically tuned climatic record from Lake Baikal, SE Siberia, Quaternary Sci. Rev., 25, 3431–3457, 2006.
Rachold, V. and Brumsack, H. J.: Inorganic geochemistry of Albian sediments from the Lower Saxony Basin NW Germany; palaeoenvironmental constraints and orbital cycles, Palaeogeogr. Palaeocl., 174, 121–143, 2001.
Rider, M. H. and Kennedy, M.: The Geological Interpretation of Well Logs, 3rd edn., Rider-French Consulting Limited, Glasgow, Scotland, 2011.
Rotolo, S. G., Scaillet, S., La Felice, S., and Vita-Scaillet, G.. A revision of the structure and stratigraphy of pre-Green Tuff ingimbrites at Pantelleria (Strait of Sicily), J. Volcanol. Geoth. Res., 250, 61–74, 2013.
Scholz, C. A., Talbot, M. R., Brown, E. T., and Lyons, R. P.: Lithostratigraphy, physical properties and organic matter variability in Lake Malawi drillcore sediments over the past, 145,000 years, Palaeogeogr. Palaeocl., 303, 38–50, 2011.
Serra, O. and Serra, L.: Well Logging and Geology, Serralog, France, 2003.
Steiger, R. H. and Jäger, E.: Subcommission on geochronology: convention on the use of decay constants in geo- and cosmochronology, Earth Planet. Sc. Lett., 36, 359–362, 1977.
Stockhecke, M., Sturm, M., Brunner, I., Schmincke, H. U., Sumita, M., Kipfer, R., Cukur, D., Kwiecien, O., and Anselmetti, F. S.: Sedimentary evolution and environmental history of Lake Van (Turkey) over the past 600 000 years, Sedimentology, 61, 1830–1861, 2014.
Sulpizio, R., Zanchetta, G., D'Orazio, M., Vogel, H., and Wagner, B.: Tephrostratigraphy and tephrochronology of lakes Ohrid and Prespa, Balkans, Biogeosciences, 7, 3273–3288, doi:10.5194/bg-7-3273-2010, 2010.
Theys, P. P.: Log data acquisition and quality control, Editions Technip, Paris, France, 1991.
Torrence, C. and Compo, G. P.: A practical guide to wavelet analysis, B. Am. Meteorol. Soc., 79, 61–78, 1998.

BGD
12, 7671–7703, 2015

Trajanovski, S., Albrecht, C., Schreiber, K., Schultheiß, R., Stadler, T., Benke, M., and Wilke, T.: Testing the spatial and temporal framework of speciation in an ancient lake species flock: the leech genus *Dina* (Hirudinea: Erpobdellidae) in Lake Ohrid, Biogeosciences, 7, 3387–3402, doi:10.5194/bg-7-3387-2010, 2010.

Vogel, H., Wagner, B., Zanchetta, G., Sulpizio, R., and Rosen, P.: A paleoclimate record with tephrochronological age control for the last glacial–interglacial cycle from Lake Ohrid, Albania and Macedonia, J. Paleolimnol., 44, 295–310, 2010a.

Vogel, H., Wessels, M., Albrecht, C., Stich, H.-B., and Wagner, B.: Spatial variability of recent sedimentation in Lake Ohrid (Albania/Macedonia), Biogeosciences, 7, 3333–3342, doi:10.5194/bg-7-3333-2010, 2010b.

Vogel, H., Zanchetta, G., Sulpizio, R., Wagner, B., and Nowaczyk, N.: A tephrostratigraphic record for the last glacial–interglacial cycle from Lake Ohrid, Albania and Macedonia, J. Quaternary Sci., 25, 320–338, 2010c.

Wagner, B., Reicherter, K., Daut, G., Wessels, M., Matzinger, A., Schwalb, A., Spirkovski, Z., and Sanxhaku, M.: The potential of Lake Ohrid for long-term palaeoenvironmental reconstructions, Palaeogeogr. Palaeocl., 259, 341–356, 2008.

Wagner, B., Wilke, T., Krastel, S., Zanchetta, G., Sulpizio, R., Reicherter, K., Leng, M., Grazhdani, A., Trajanovski, S., Levkov, Z., Reed, J., and Wonik, T.: More than one million years of history in lake Ohrid Cores. EOS, transactions, American Geophysical Union, 95, 25–32, 2014.

Weedon, G.: Time-Series Analysis and Cyclostratigraphy, Examining Stratigraphic Records of Environmental Cycles, Cambridge University Press, Cambridge, UK, 2003.

Wonik, T.: Gamma-ray measurements in the Kirchrode I and II boreholes, Palaeogeogr. Palaeocl., 174, 97–105, 2001.

Wu, H., Zhang, S., Feng, Q., Jiang, G., Li, H., and Yang, T.: Milankovitch and sub-Milankovitch cycles of the early Triassic Daye Formation, South China and their geochronological and paleoclimatic implications, Gondwana Res., 22, 748–759, 2012.

BGD
12, 7671–7703, 2015

Table 1. The downhole logging data correlated to LR04 (Lisiecki and Raymo, 2005). Eight anchor points from tephrochronology and 30 additional tie points of significant features between the downhole data and LR04 are set. The tephra ages were recalculated (except Y-3) according relative to ACs-2 at 1.193 Ma (Nomade et al., 2005) and the total decay constant of Steiger and Jäger (1977), uncertainties are 2δ. mblf – metres below lake floor.

depth mblf	age (LR04) ka	age (tephra pointer) ka	correlated eruption/tephra	reference
1.46	4			
13.67		29	Y-3	Albert et al. (2014)
19.35		39	Y-5 (Campanian Ignimbrite)	De Vivo et al. (2001)
24.37	49			
30.17	62			
36.41	78			
40.10	87			
48.40		109 ± 2	X-6	Iorio et al. (2013)
55.11		129 ± 6	P11	Rotolo et al. (2013)
59.19	140			
66.73		162 ± 6	Vico B	Laurenzi and Villa (1987)
74.61	171			
85.09	185			
97.00	206			
103.40	223			
106.48	230			
112.10	246			
121.75	271			
132.92	294			
144.00	317			
150.65	342			
153.76	350			
161.52	374			
167.80	392			
170.04	398			
178.29	433			
183.28	456	457 ± 2	Pozzolane Rosse	Giaccio et al. (2013)
201.31	508			
203.05		511 ± 6	Acerno A10-A9	Petrosino et al. (2014)
206.70		527 ± 2	Tufo Bagni Albule	Marra et al. (2009)
209.09	536			
212.89	549			
215.53	557			
219.20	568			
220.99	574			
225.44	585			
240.00	630			

BGD
12, 7671–7703, 2015

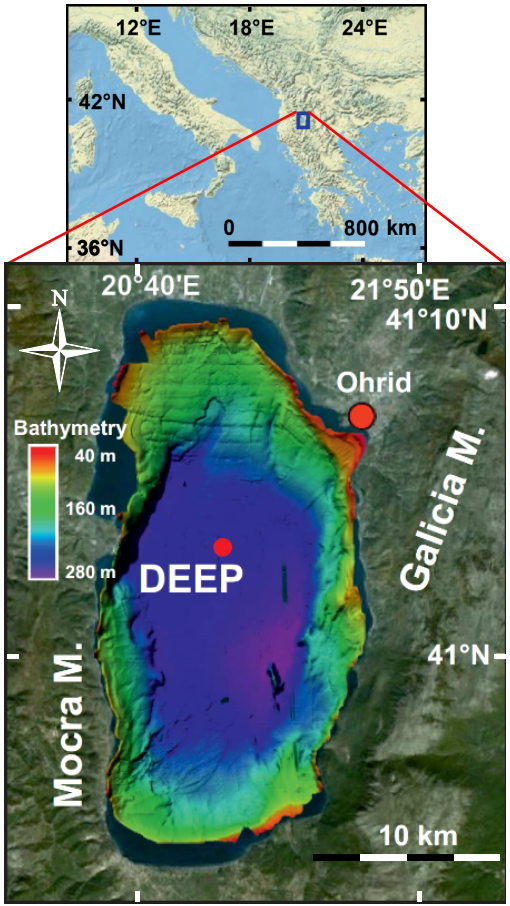

Figure 1. Regional and bathymetric map of Lake Ohrid (modified after Wagner et al., 2014). The city of Ohrid and the DEEP drill sites from the ICDP campaign in spring 2013 are shown.

BGD
12, 7671–7703, 2015

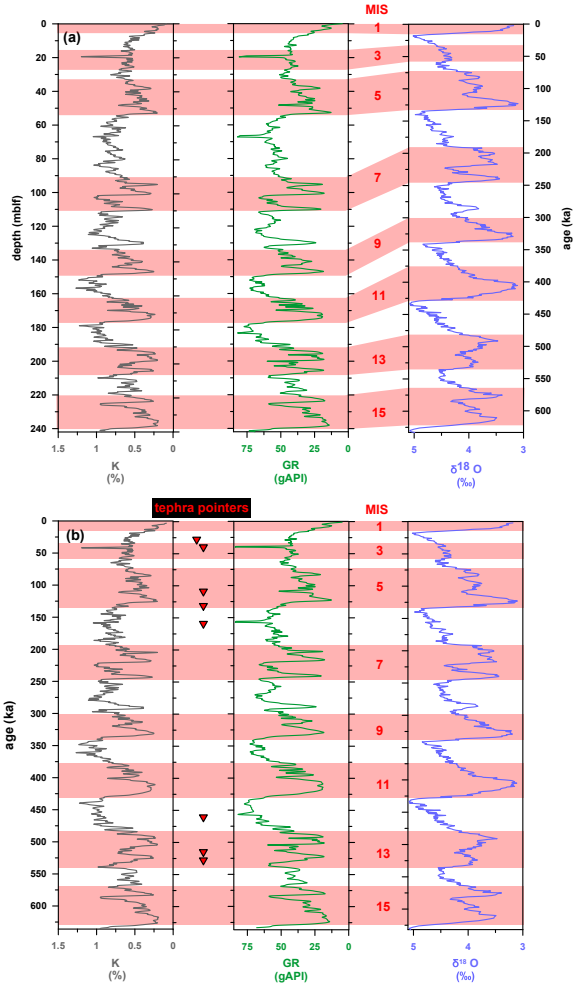

BGD
12, 7671–7703, 2015

Age depth-model for the past 630 ka in Lake Ohrid

H. Baumgarten et al.

Figure 2. (a) Correlation of downhole GR and K data from 0 to 240 mblf with LR04 (Lisiecki and Raymo, 2005) from 0 to 630 ka. The depth age-range was set by eight anchor points from tephrochronology. Warm and/or humid periods correlate with periods of low GR and K values. K – potassium content from spectral gamma ray, GR – total gamma radiation, MIS – Marine Isotope Stages, mblf – metres below lake floor. **(b)** An age scale was applied to the downhole logging data (GR and K) based on tie points to LR04 (Lisiecki and Raymo, 2005) and age marker points from tephrochronology. K – potassium content from spectral gamma ray, GR – total gamma radiation, MIS – Marine Isotope Stages, mblf – metres below lake floor.

BGD
12, 7671–7703, 2015

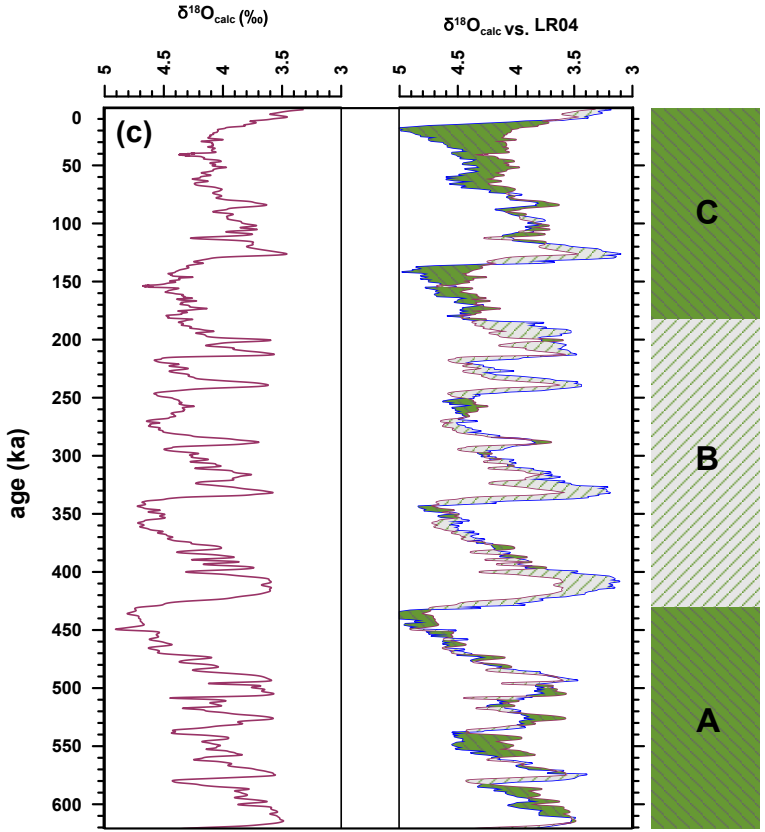

Figure 2. (c) A synthetic curve calculated by simple linear regression between GR on age scale and LR04. Both curves are displayed as overlay. Three zones are identified. (A) 630 to 430 ka (MIS 15 to 12), (B) 430 to 185 ka (MIS 11 to 7) and, (C) 185 to 0 ka (MIS 6 to 1). $\delta^{18}O_{calc}$ is prevailing decreased during zones (A) and (C) (dark green colour) and higher in zone (B) (light green colour) compared to LR04.

BGD
12, 7671–7703, 2015

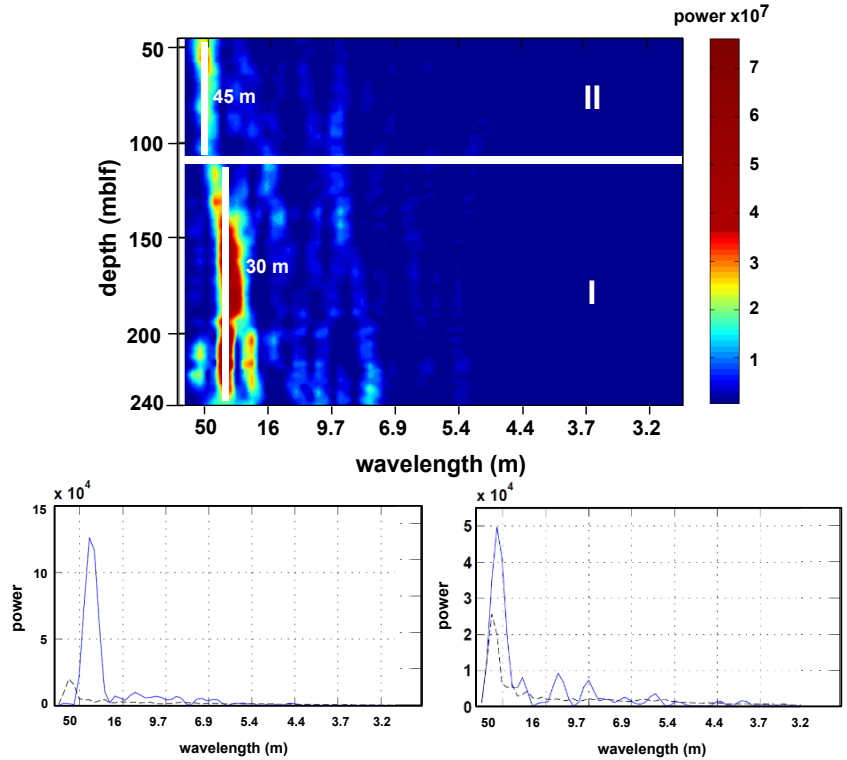

Figure 3. Three-dimensional spectrogram from sliding window analysis of GR data from 0 to 240 mblf. The relative power of the frequency components is indicated by colour and two spectral peaks with wavelengths of 30 and 45 m are apparent. Based on the break in the spectral characteristics at about 110 mblf, the spectral plot was subdivided into a lower interval I (240 to 110 mblf) and an upper interval II (110 to 0 mblf). Two single spectrum of GR within interval I at 170 mblf (left) and interval II at 50 mblf (right) are displayed below. The emphasized wavelengths of 30 m for interval I and 45 m for interval II are prominent in the single spectra.

BGD
12, 7671–7703, 2015

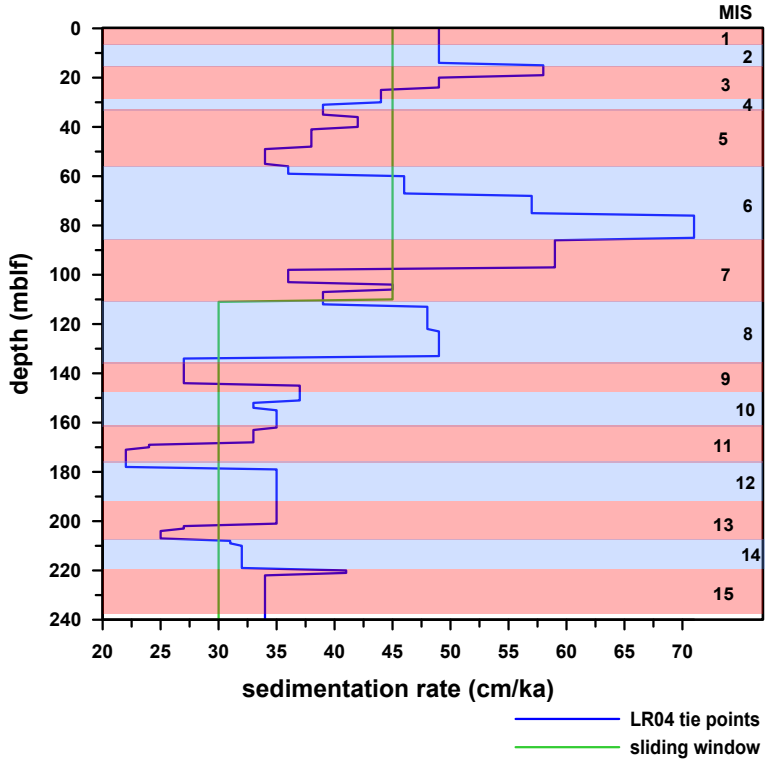

Figure 4. Estimates of sedimentation rates from 0 to 240 mblf based on visual correlation and tying to LR04 (blue; Lisiecki and Raymo, 2005) and sliding window analysis and linking of high amplitudes to the 100 ka cycle (green). The sedimentation rates from sliding window analysis show an increase from 30 to 45 cm ka^{-1} at about 110 mblf, whereas results from tie points are more variable and range from 22 to 71 cm ka^{-1}. MIS stages from MIS 1 to 15 are indicated. MIS – Marine Isotope Stages, mblf – metres below lake floor.

BGD
12, 7671–7703, 2015

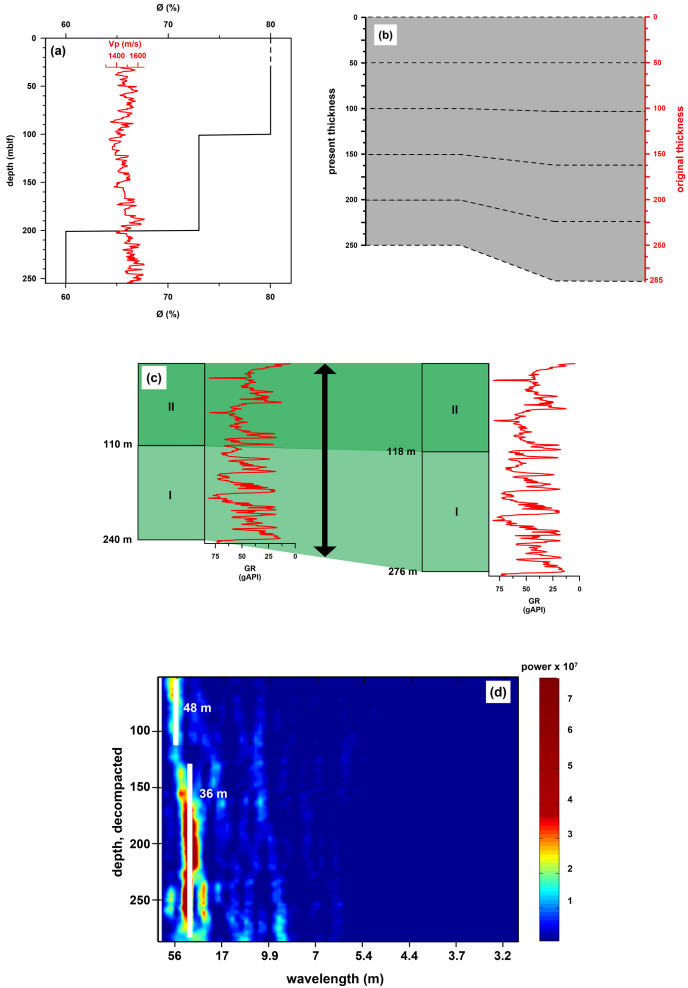

BGD
12, 7671–7703, 2015

Age depth-model for the past 630 ka in Lake Ohrid

H. Baumgarten et al.

Figure 5. (a) Porosity values derived from sonic (Vp) after Erickson and Jarrard (1998) from 30 to 250 mblf. Average values for intervals of 100 m length were calculated as indicated by the black line and values for the top 30 m of the sediments were linear interpolated (dashed line). The initial porosity (surface porosity) of 80 % was used for modeling of compaction by 2-D Move. ϕ – porosity, Vp – p wave velocity from sonic, mblf – metres below lake floor. **(b)** Sediment layers of thicknesses of 50 m are modelled by use of the software 2-D Move. From a present thickness of 250 m, the original thickness after decompaction of the sediment column was estimated at 285 m. **(c)** The GR data from 0 to 240 mblf and the intervals from subdivision by spectral characteristics at about 110 mblf (left). The data was stretched to the estimates of the original thicknesses of the sediment layers and the resulting increased lengths of GR and new interval borders are displayed (right). **(d)** Result from sliding window analysis of stretched GR data. Two spectral peaks with wavelengths of 36 and 48 m are emphasized.

BGD
12, 7671–7703, 2015

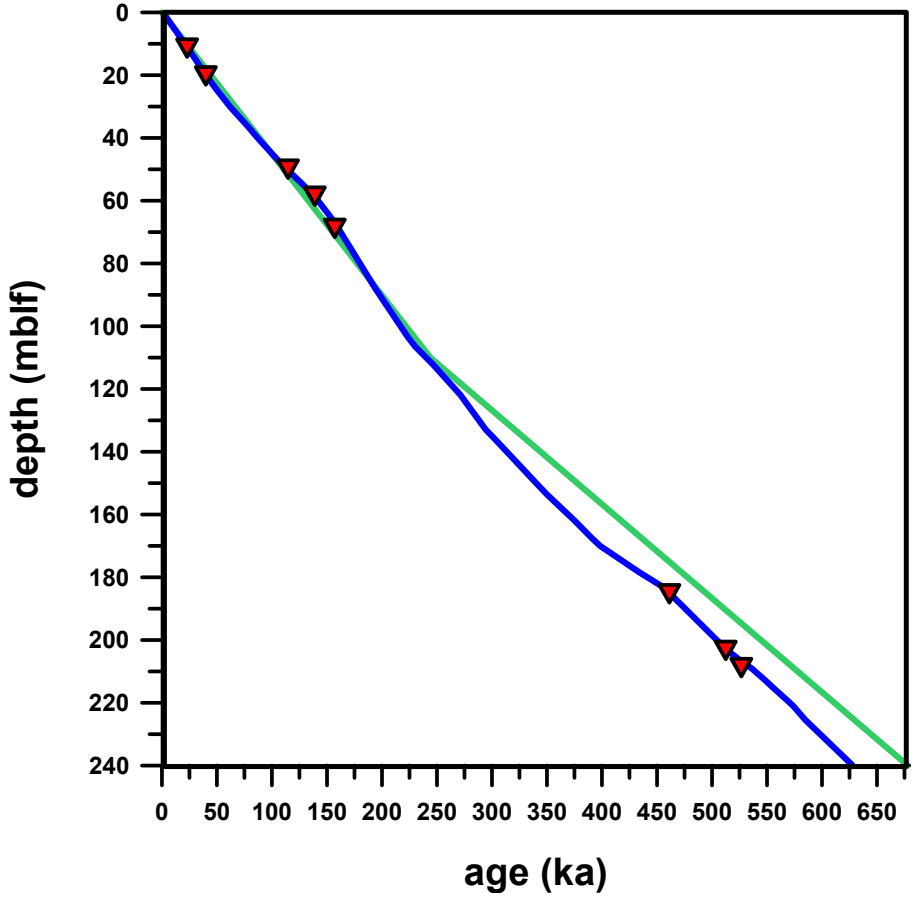

Figure 6. Depth age-model for the sediment depths of 0 to 240 mblf. The two curves were generated by visual tying to LR04 (blue; Lisiecki and Raymo, 2005) and by linking of prominent cycles to the 100 ka signal (green). Tephra pointers are indicated by red triangles.

BGD
12, 7671–7703, 2015